ACS SENSORS

pubs.acs.org/acssensors Article

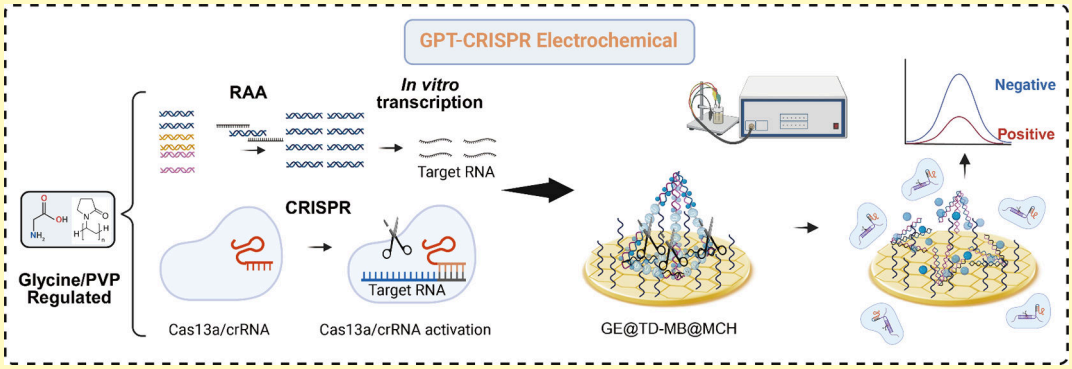
Glycine/PVP-Enabled One-Pot CRISPR/Cas13a Detection of *Vibrio parahaemolyticus* by Tetrahedron-Mediated Electrochemistry

Published as part of ACS Sensors special issue "CRISPR in Sensing".

Jincheng Zhang,† Shuang Liang,† Yue Sun, Cuixing Zhan, Gan Xue, and Xin Zhou*

Cite This: https://doi.org/10.1021/acssensors.6c00902 Read Online

ACCESS | Metrics & More | Article Recommendations | Supporting Information



ABSTRACT: *Vibrio parahaemolyticus* is a major foodborne pathogen widely distributed in aquatic environments and seafood supply chains, necessitating rapid and ultrasensitive detection strategies adaptable to diverse testing scenarios. Here, we present a glycine/ PVP- and tetrahedron-integrated one-pot CRISPR sensing platform (termed GPT-CRISPR) for robust and ultrasensitive nucleic acid detection. The platform introduces chemical regulation into a multienzyme one-pot RAA−CRISPR/Cas13a network, where glycine may help reduce nonspecific Cas13a background activity, possibly through weak competitive interactions, while polyvinylpyrrolidone (PVP) may enhance reaction compatibility through macromolecular crowding and spatial shielding. This coordinated microenvironment enables stable amplification and CRISPR activation within a single closed vessel while minimizing background interference. Upon target recognition, activated Cas13a cleaves uracil-containing, surface-immobilized DNA tetrahedra, translating molecular recognition into amplified electrochemical signals. This transduction strategy enables quantitative detection with a linear dynamic range of 1.5 to 3×10^3 copies μL^{-1} and a limit of detection of 0.38 copies μL^{-1}. The same chemically regulated one-pot CRISPR framework remains compatible with fluorescence and lateral flow readouts. The assay operates under isothermal conditions and delivers results within 30 min without complex sample preparation. Validation across real-world samples demonstrates robustness in complex matrices. Collectively, GPT-CRISPR integrates chemical stabilization of a one-pot CRISPR framework with electrochemical transduction, defining a robust sensing architecture with adaptable readout capability.

KEYWORDS: *Vibrio parahaemolyticus, chemical regulation, one-pot CRISPR, tetrahedron, electrochemical biosensing*

Vibrio parahaemolyticus is a Gram-negative halophilic bacterium widely distributed in marine and estuarine environments and is a leading cause of seafood-borne gastroenteritis worldwide.[1,2] Infection through contaminated seafood can result in gastrointestinal illness and, in severe cases, septicemia, posing a persistent threat to food safety and public health.[3,4] The increasing prevalence of *Vibrio parahaemolyticus* in aquaculture and food products highlights an urgent need for rapid, sensitive, and deployable detection technologies. Current detection methods for *Vibrio parahaemolyticus* include culture-based assays, immunological methods,[5] and nucleic acid-based diagnostics,[6] such as qPCR,[7] CRISPR-associated/derived assays,[8−10] and isothermal amplification.[11] Although these approaches have been widely reported and applied, they are often limited by a long assay time, instrumentation dependence, insufficient sensitivity, or susceptibility to nonspecific signals in complex matrices. Therefore, more robust and practical diagnostic strategies remain highly desirable. Our previously developed visualization-based

Received: March 1, 2026
Revised: May 6, 2026
Accepted: May 22, 2026

ACS Publications © XXXX American Chemical Society

detection strategies for *Vibrio parahaemolyticus* using engineered phage probes were combined with DFM.[12] However, the reliance on imaging instrumentation and susceptibility to matrix interference underscore the need for molecular-level sensing platforms with improved robustness and broader applicability.

In this context, CRISPR-based molecular diagnostics have rapidly emerged as a versatile class of nucleic acid detection technologies, owing to the programmable recognition and collateral cleavage activities of CRISPR-associated enzymes.[13,14] Both Cas12 and Cas13 systems have been extensively engineered to develop diverse sensing strategies, including amplification-free assays, preamplification-assisted formats, target preconcentration schemes, crRNA engineering for differential activation, and reaction network optimization through modulation of Cas−crRNA interactions.[15] In parallel, substantial efforts have been devoted to signal readout innovation, leading to a broad spectrum of visualization and detection modalities such as lateral flow strips,[16] microfluidic platforms,[17] portable devices,[18] and even automated result interpretation based on machine learning and convolutional neural networks.[19] Despite these advances, many CRISPR-based assays still suffer from intrinsic limitations, including complex multistep workflows,[20] susceptibility to contamination in two-step formats,[21] high probe or reagent cost,[22] and insufficient robustness across heterogeneous application scenarios.[23] In particular, the incompatibility among multiple enzymes in integrated one-pot systems often compromises reaction efficiency and analytical sensitivity.[15,24] Recent studies have highlighted the potential of chemical regulation strategies to address these challenges, where various additives such as polyols, polymers, amine-containing compounds, and metal-ion-derived solvent modifiers have been introduced to stabilize proteins and/or modulate the physicochemical properties of reaction media, thereby influencing enzymatic kinetics and system performance.[25−27] These findings suggest that chemical additive-assisted regulation is promising for improving the robustness and sensitivity of one-pot CRISPR diagnostics. Nevertheless, signal transduction strategies that can simultaneously achieve high sensitivity, quantitative output, operational simplicity, and compatibility with complex real-world matrices remain insufficiently developed. Collectively, these challenges highlight the need for improved CRISPR diagnostic architectures that integrate simplified one-pot operation with enhanced signal fidelity and practical deplorability.

Electrochemical sensing represents a highly promising approach for the development of practical point-of-care testing (POCT) systems, owing to its high sensitivity, quantitative capability, miniaturization potential, and compatibility with portable instrumentation.[28−30] Nevertheless, directly coupling CRISPR collateral cleavage activity to reliable electrochemical outputs remains challenging, largely due to nonspecific adsorption, uncontrolled probe orientation, and signal instability at the electrode interface.[31−34] Rational engineering of the sensing interface is therefore essential for achieving robust and reproducible electrochemical CRISPR diagnostics. In this context, DNA tetrahedra (TD) have emerged as well-defined three-dimensional nanostructures for constructing highly ordered biosensing interfaces.[35−37] DNA TD exhibit a rigid architecture and nanoscale dimensions and can be conveniently assembled with high yield through programmable self-assembly.[38] Importantly, their geometrically defined structure enables precise spatial presentation of functional probes and effective suppression of nonspecific surface interactions when immobilized on electrode surfaces.[39,40] These characteristics make DNA TD particularly suitable as interfacial scaffolds for organizing CRISPR-responsive probes and enhancing the efficiency and reliability of electrochemical signal transduction.

In this work, we introduce a chemically regulated one-pot CRISPR sensing framework that integrates glycine/PVP-enabled coordination of a multienzyme reaction network with a surface-engineered electrochemical interface. Rather than relying solely on reaction optimization or readout enhancement, this strategy establishes cooperative regulation between molecular amplification, CRISPR activation, and signal transduction within a single closed system. By stabilizing enzyme compatibility at the reaction level and structuring signal conversion at the interface level, GPT-CRISPR resolves two central challenges in practical CRISPR biosensing: maintaining reaction robustness in one-pot formats and achieving quantitative electrochemical transduction with reduced interfacial variability. Importantly, the molecular recognition framework remains modular, allowing alternative output formats without altering the core reaction chemistry. This integrated design provides a unified yet adaptable sensing architecture for pathogen detection in heterogeneous matrices.

EXPERIMENTAL SECTION

Detailed descriptions of the reagents and instruments, strain preparation, one-pot CRISPR optimization, establishment of the glycine/PVP-enabled one-pot CRISPR framework, optimization of the TD-mediated electrochemical interface, integration with LFA detection, electrochemical performance evaluation, and methodological validation in real samples are provided in the Supporting Information.

RESULTS AND DISCUSSION

Design Principle of a GPT-CRISPR Sensing Platform for Ultrasensitive Detection of *Vibrio parahaemolyticus*

We developed a platform termed GPT-CRISPR for rapid and ultrasensitive detection of *Vibrio parahaemolyticus*, in which RAA is seamlessly coupled with programmable CRISPR-based signal transduction and a tetrahedron-modified gold electrode enables quantitative electrochemical readout. As illustrated in Figure 1, the incorporation of glycine and PVP stabilizes the multienzyme reaction network, enabling robust one-pot operation while minimizing manual handling and reducing the risk of cross-contamination. In addition, we constructed a TD-mediated electrochemical interface that establishes a well-defined sensing architecture, suppresses nonspecific adsorption, and improves analytical robustness and quantitative performance. Upon target recognition, Cas13a-mediated collateral cleavage triggers the release of embedded MB reporters, resulting in a measurable electrochemical signal change. The same one-pot CRISPR framework also supports fluorescence and LFA readouts, allowing flexible deployment across laboratory, field, and point-of-need settings. The workflow consists of rapid sample pretreatment (∼5 min), a GPT-CRISPR reaction (∼20 min), and optional fluorescence or LFA readout (∼2 min), allowing completion within approximately 27 min.

Optimization of RAA Amplification and CRISPR/Cas13a Cleavage Conditions

To ensure sufficient sensitivity for detecting low-abundance *Vibrio parahaemolyticus* in complex matrices, we adopted nucleic acid preamplification as a foundational step for the CRISPR/Cas13a assay. Although amplification-free CRISPR strategies have been reported,[15] their performance in real samples is often

https://doi.org/10.1021/acssensors.6c00902
ACS Sens. XXXX, XXX, XXX-XXX

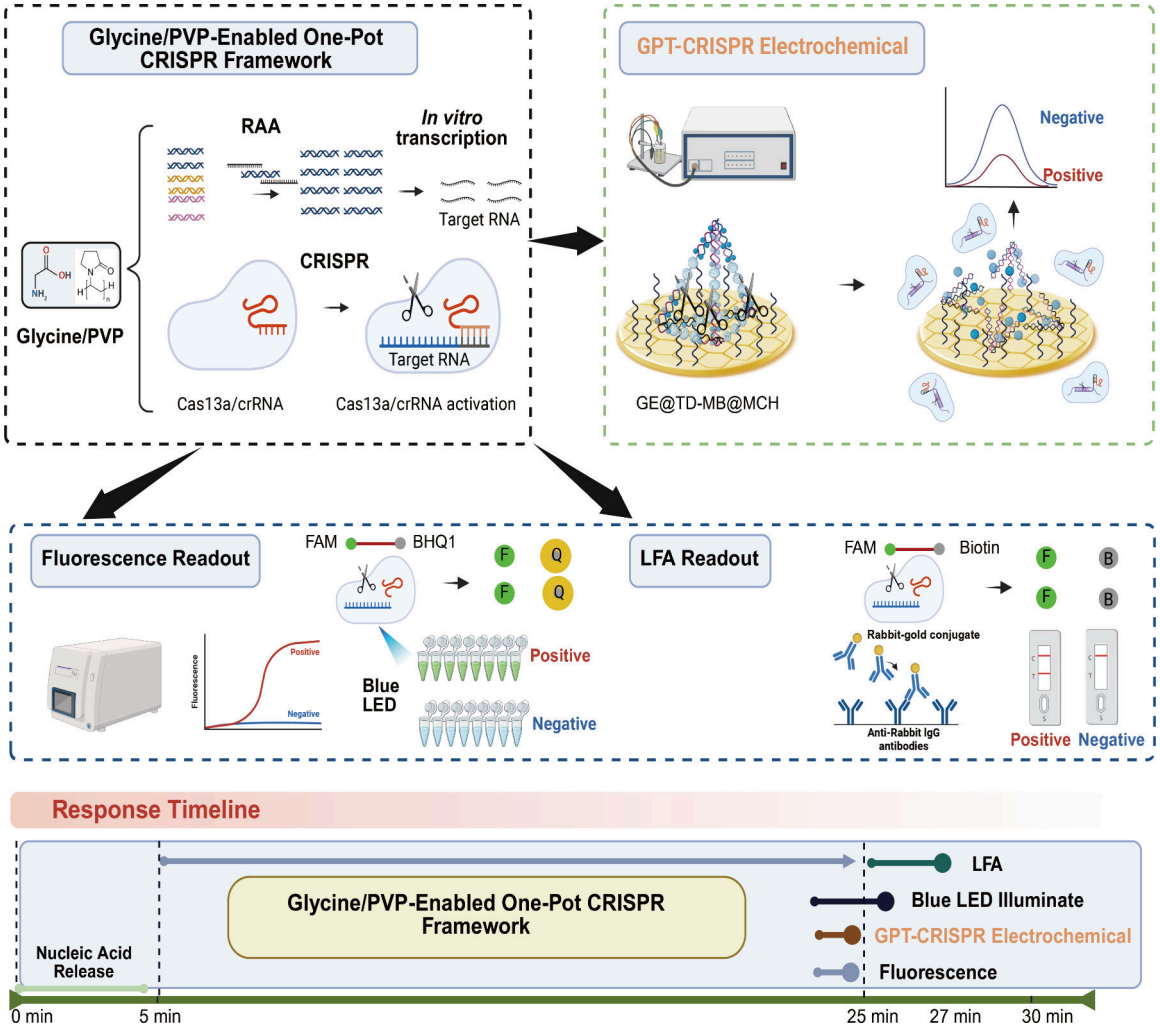


Figure 1. Schematic illustration and assay timeline of the GPT-CRISPR electrochemical sensing platform for *Vibrio parahaemolyticus*. The assay integrates RAA, T7-mediated *in vitro* transcription, and Cas13a collateral cleavage into a single isothermal reaction enabled by glycine/PVP-mediated chemical regulation. Following rapid sample pretreatment and nucleic acid release, target DNA is amplified by RAA using primers containing a T7 promoter. The resulting amplicons are transcribed in situ to generate target RNA, which activates the Cas13a−crRNA complex and triggers collateral cleavage of reporters within the same reaction vessel. In the GPT-CRISPR configuration, Cas13a activity is primarily transduced through a TD-engineered electrochemical interface, enabling quantitative electrical signal readout. Within the same one-pot CRISPR framework, fluorescence and LFA are additionally supported as complementary readout options for scenario-specific visualization and deployment. Schematic illustrations were created using BioRender.com.

constrained by limited target copy numbers and susceptibility to background interference. RAA was selected because of its rapid kinetics and low operating temperature, which make it a suitable amplification module for integration with CRISPR-based detection.[41] However, direct integration of RAA with Cas13a cleavage is often hampered by enzymatic incompatibility and reaction interference. Therefore, we first optimized key assay parameters using a two-step RAA−CRISPR/Cas13a format and subsequently improved reaction compatibility during the construction of the one-pot system.

Primer performance was first evaluated, and 10 primer pairs targeting the *VPA1585* gene were designed for screening. Agarose gel electrophoresis showed that the primer pair RAA-1-Fw/Rv generated the strongest and most specific amplification band (Figure S1A). Using this primer pair, reaction temperature and incubation time were systematically optimized. The highest amplification efficiency was obtained at 43 °C with a reaction time of 25 min, as evidenced by increased band intensity and quantitative grayscale analysis (Figure S1B,C). In addition, the sensitivity of the optimized RAA assay was evaluated, and the method was able to detect as low as 3×10^2 copies μL^{-1} of target DNA (Figure S1D).

Based on the RAA-1 amplicon sequence, four crRNAs were designed and evaluated using *in vitro* transcribed RNA targets. Kinetic fluorescence analysis showed that crRNA-1 exhibited the strongest cleavage activity and the fastest response among the candidates (Figure S2A) and was therefore selected for subsequent experiments. Finally, key components of the CRISPR/Cas13a system were systematically optimized to improve reaction efficiency and analytical sensitivity. Individual variation of crRNA, Cas13a protein, and ssRNA reporter concentrations revealed that optimal performance, balancing sensitivity and economy, was achieved with 12 nM crRNA, 50 ng Cas13a, and 40 μM reporter (Figure S2B−D). In addition, the amounts of T7 RNA polymerase and rNTP were further optimized, showing that 0.25 μL of T7 RNA polymerase and 8 nM rNTP provided the most efficient transcription cleavage coupling and fastest signal

https://doi.org/10.1021/acssensors.6c00902
ACS Sens. XXXX, XXX, XXX-XXX

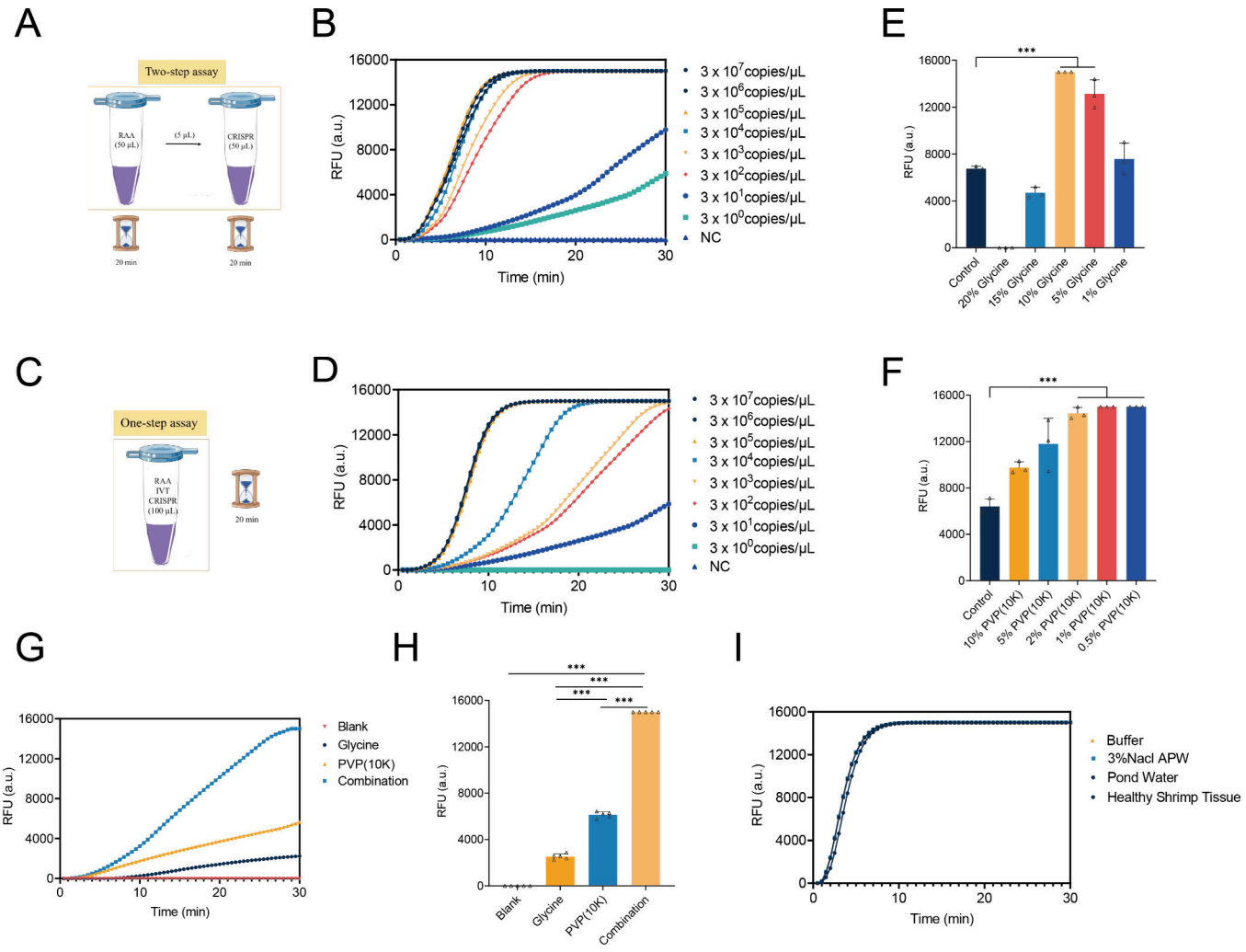


Figure 2. Feasibility validation of the glycine/PVP-enabled one-pot assay. (A, B) Sensitivity analysis of the two-step RAA−CRISPR/Cas13a assay. (C, D) Sensitivity analysis of the one-pot RAA−CRISPR/Cas13a assay obtained by directly integrating the optimized two-step conditions into a single tube. (E, F) Evaluation of the effects of chemical additives on assay performance using 3×10^1 copies μL^{-1} of target DNA, showing the influence of different concentrations of glycine (E) and PVP (10 kDa) (F) on signal enhancement. (G, H) Evaluation of assay performance using 3 copies μL^{-1} of target DNA in the absence of additives, with glycine alone, PVP (10 kDa) alone, or their combination, shown as fluorescence kinetics (G) and endpoint signal comparison (H). (I) Stability of the glycine/PVP-enabled one-pot assay in complex matrices. Statistical analysis was performed using one-way ANOVA in GraphPad Prism 8. Significance levels are indicated as ns, $P > 0.05$; $^*P \leq 0.05$; $^{**}P \leq 0.01$; $^{***}P \leq 0.001$.

generation (Figure S2E,F). These optimized parameters were subsequently applied to the construction and evaluation of the one-pot RAA−CRISPR/Cas13a detection platform.

Sensitivity of the Glycine/PVP-Enabled One-Pot Framework Comparable to the Two-Step Workflow

Under the optimized conditions established, a two-step RAA−CRISPR/Cas13a assay was first constructed by separating RAA amplification from the subsequent T7-mediated transcription and Cas13a cleavage reaction. As shown in Figure 2A,B, this configuration exhibited high analytical sensitivity toward target DNA. Specifically, target concentrations ≥3 copies μL^{-1} generated fluorescence signals significantly above the background level, confirming the sensitivity of the two-step workflow. To further simplify operation and reduce overall assay time, we subsequently integrated all components into a single-tube one-pot format, in which RAA amplification, *in vitro* transcription, and Cas13a-mediated collateral cleavage proceeded concurrently under isothermal conditions. However, direct integration of the two optimized reaction modules led to a pronounced loss of sensitivity. As shown in Figure 2C,D, the limit of detection of the one-pot system was approximately 10-fold poorer than that of the two-step assay, despite using the same optimized reaction components. This performance deterioration is consistent with previous reports and can be attributed to enzyme incompatibility, competition among reaction components, and elevated background activity in complex multienzyme reaction networks.[42]

On this basis, we investigated whether chemical additives could improve one-pot reaction performance. Glycine and polyvinylpyrrolidone (PVP, 10 kDa), two additives previously reported to enhance enzymatic reactions, were therefore selected for further evaluation.[26,27] As shown in Figure 2E and Figure S3A, supplementation with glycine alone improved the performance of the one-pot system when challenged with 3×10^1 copies μL^{-1} of target DNA. Among the glycine concentrations tested, 10% glycine produced the strongest signal enhancement and enabled the fluorescence signal to reach the plateau level. This result indicates that glycine contributes positively to the functional performance

https://doi.org/10.1021/acssensors.6c00902
ACS Sens. XXXX, XXX, XXX-XXX

of the one-pot assay. A possible explanation is that glycine, as a classical zwitterionic small molecule,[43] may weakly modulate the local microenvironment around proteins and nucleic acids through hydration-mediated interactions and subtle effects on conformational equilibrium.[44,45] In the context of Cas13a, glycine may help reduce nonspecific background activity in the nonactivated state by weakly stabilizing the catalytic system, thereby making spontaneous collateral cleavage less favorable. Once target recognition triggers the correct conformational activation, this weak inhibitory effect may be overcome. Notably, our experimental results also show that glycine enhances the overall fluorescence output of the one-pot system, indicating that its net effect is to improve assay performance rather than simply inhibit enzyme activity. This behavior is consistent with reduced background interference together with enhanced effective output of the cascade reaction. Therefore, the observed effect of glycine is consistent with suppression of nonspecific Cas13a background activity, although this interpretation remains a plausible mechanistic hypothesis rather than direct molecular proof.

Similarly, supplementation with PVP alone also improved the performance of the one-pot assay (Figure 2F). Both 1% and 0.5% PVP enabled the fluorescence signal to approach the plateau level, although 1% PVP reached the plateau more rapidly than 0.5% PVP (Figure S3B), indicating improved assay performance within an appropriate concentration range. While the present results do not provide direct mechanistic evidence, this concentration-dependent effect is consistent with the reported physicochemical properties of PVP-10k as a polymeric crowding additive.[46] PVP may therefore contribute to improved one-pot assay performance by modulating the local reaction environment and enhancing compatibility among the multiple enzymatic steps.[47,48] Notably, the beneficial effect of PVP was concentration-dependent rather than monotonic, supporting the view that its action is related to optimization of the reaction microenvironment rather than simple signal enhancement.

Encouraged by these results, we next investigated whether glycine and PVP could act cooperatively in the one-pot system. Under the same challenge condition of 3 copies μL^{-1} target DNA, 10% glycine, 1% (w/v) PVP, or their combination all generated detectable fluorescence signals (Figure 2G). However, only the combined condition enabled the fluorescence signal to reach the plateau level (Figure 2H), indicating a cooperative functional effect. In addition, the regulatory effects of glycine and PVP showed no significant variation across the different sample matrices, suggesting that their performance was not substantially affected by matrix interference (Figure 2I). This behavior is consistent with complementary contributions of glycine and PVP to one-pot assay performance, although the underlying mechanism remains to be established.

TD-Mediated Electrochemical Performance of the One-Pot CRISPR Assay

To further improve analytical robustness and quantitative performance, the TD-mediated electrochemical interface was integrated into the one-pot CRISPR framework. As schematically shown in Figure 3A, the TD nanostructure functions as a well-defined scaffold to spatially organize redox reporters on the electrode surface while minimizing nonspecific adsorption, thereby enabling efficient transduction of Cas13a activity into electrical signals. Native PAGE confirmed successful TD assembly, as evidenced by the stepwise mobility shift upon sequential addition of strands S1−S4 (Figure 3B). DLS analysis revealed a narrow size distribution with an average hydrodynamic diameter of 10.98 nm and a zeta potential of approximately −30 mV (Figure S4A,B), consistent with typical DNA nanostructures. TEM analysis further confirmed the successful formation of monodisperse and structurally well-defined TD (Figure 3C). The TD probes were immobilized onto gold electrodes via Au−S bonds to construct the sensing interface. Electrochemical measurements revealed stepwise changes corresponding to each surface modification. Compared with the bare electrode, TD immobilization led to a clear decrease in redox peak currents and an increase in charge-transfer resistance, consistent with the introduction of an insulating DNA layer. Subsequent passivation with mercaptohexanol (MCH) further amplified this blocking effect, confirming successful surface backfilling (Figure 3D,E). After loading MB, additional changes in the electrochemical responses were observed, indicating the successful incorporation of the redox reporter into the TD-modified interface.

To verify that the TD could serve as a Cas13a-responsive substrate, trans-cleavage experiments were performed. As illustrated in the schematic model, the intact TD remained structurally stable in the presence of Cas13a or Cas13a−crRNA complexes alone, whereas addition of the target RNA triggered Cas13a activation and selective cleavage of the uracil-containing TD strands (Figure 3F). This native PAGE result confirms that TD serves as an effective trans-cleavage substrate for Cas13a (Figure 3G). Electrochemical signal transduction was further evaluated using the TD-modified sensing interface. In the absence of the target, the intact TD structure retained abundant MB molecules on the electrode surface, resulting in strong electrochemical responses. Upon target recognition, activation of Cas13a triggered trans-cleavage of the TD strands, leading to TD disassembly and the release of MB from the electrode interface. This process produced a pronounced decrease in peak current accompanied by corresponding changes in impedance, clearly distinguishing target-positive samples from controls (Figure 3H−J).

Performance Evaluation of the GPT-CRISPR Sensing Platform with Electrochemical Readouts

The analytical performance of the proposed platform was systematically evaluated using the TD-mediated electrochemical readout, which showed strong quantitative capability and high sensitivity. Under the optimized conditions, serial dilutions of the VPA1585 plasmid standard were analyzed to construct the calibration curve. The electrochemical peak current exhibited a clear concentration-dependent response, and a linear relationship between the signal change (ΔI) and the logarithm of target concentration was observed (Figure 4A). The resulting calibration curve yielded the regression equation $Y = -4.499X + 29.88$ with a correlation coefficient of $R^2 = 0.9495$, and the linear dynamic range was 1.5 to 3×10^3 copies μL^{-1} (Figure 4C). The limit of detection (LoD) was determined to be 0.38 copies μL^{-1}, which was approximately one order of magnitude lower than that of the fluorescence-based one-pot assay (3 copies μL^{-1}), highlighting the sensitivity advantage of the electrochemical transduction format. Notably, this sensitivity is also at least one order of magnitude better than that reported in a recent study employing a conventional one-pot RPA−CRISPR/Cas12a system combined with microfluidic detection for *Vibrio parahaemolyticus*.[49]

To further validate the applicability and robustness of this plasmid-based calibration in biologically relevant samples, *Vibrio parahaemolyticus* cultures were serially diluted, and genomic DNA

https://doi.org/10.1021/acssensors.6c00902
ACS Sens. XXXX, XXX, XXX-XXX

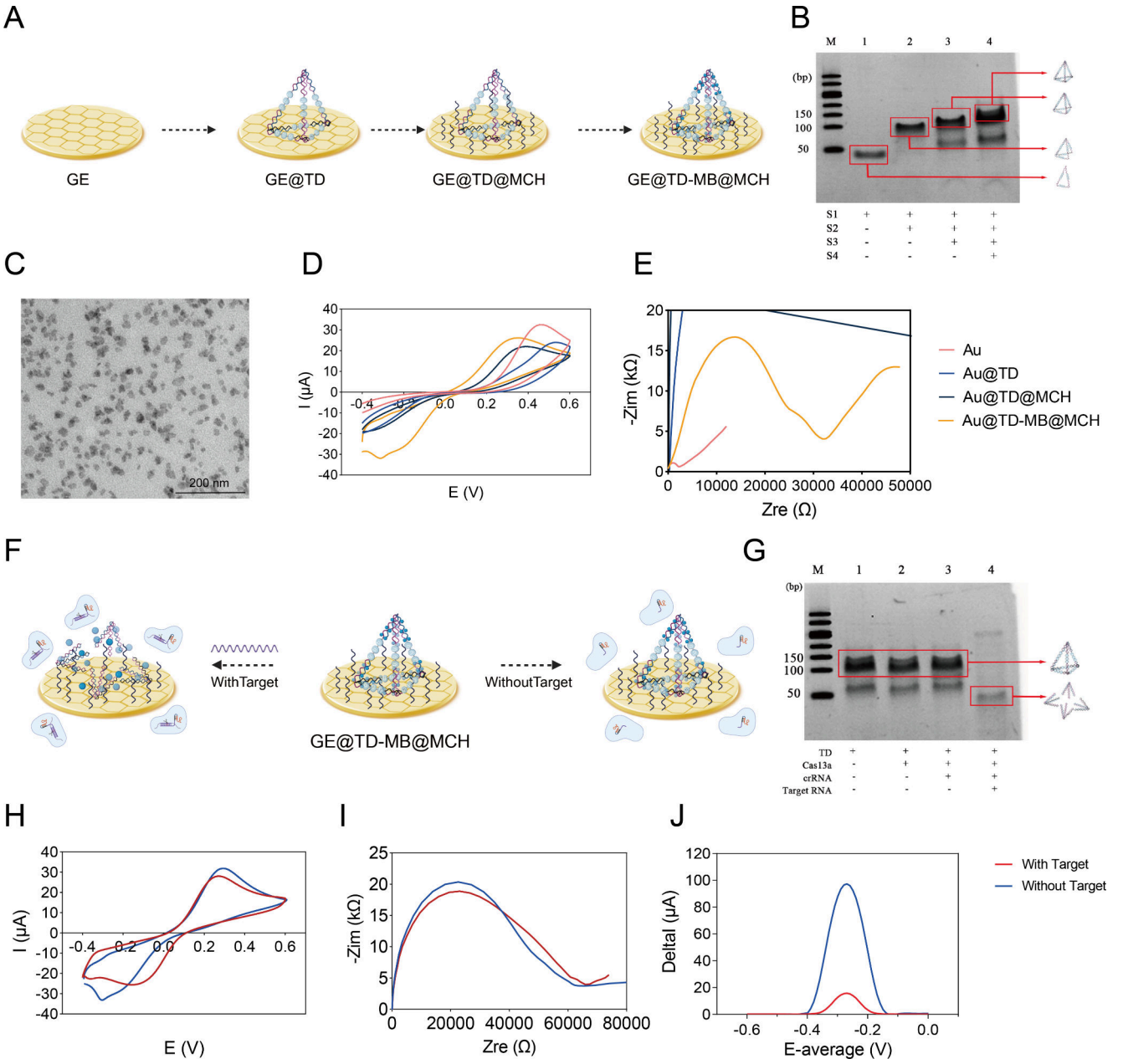


Figure 3. Characterization of the TD-mediated electrochemical interface and Cas13a-responsive signal transduction. (A) Schematic illustration of TD assembly and modification of the gold electrode surface for electrochemical sensing. (B) 10% Native PAGE analysis showing stepwise TD assembly from strands S1−S4 (M: marker; 1: S1; 2: S1 + S2; 3: S1 + S2 + S3; 4: S1 + S2 + S3 + S4). (C) TEM characterization of TD assembly. (D, E) Cyclic voltammetry (CV) and electrochemical impedance spectroscopy (EIS) responses of the electrode at different modification stages (bare GE, TD-modified GE, MCH-passivated GE, and MB-loaded TD interface). (F) Schematic illustration of TD cleavage by activated Cas13a. (G) Native PAGE analysis of Cas13a-mediated trans-cleavage of TD in the presence of target RNA (M: DNA marker; 1: TD; 2: TD + crRNA; 3: TD + crRNA + Cas13a; 4: TD + crRNA + Cas13a + target RNA). (H−J) Electrochemical responses of the TD-modified interface before and after Cas13a activation, including CV (H), EIS (I), and square wave voltammetry (SWV) (J).

was then extracted from each dilution for GPT-CRISPR analysis. Positive signals were obtained over the range of 10^1−10^6 CFU/mL (Figure S5A). Moreover, within 10^2−10^5 CFU/mL, the GPT-CRISPR signals showed a good linear relationship, yielding the regression equation $Y = -3.958X + 34.17$ with $R^2 = 0.9590$ (Figure S5B). In addition, the GPT-CRISPR results showed a strong correlation with the genomic copy numbers determined by qPCR, with a Pearson's correlation coefficient of 0.9885 (Figure 4D).

To further evaluate the contribution of the interfacial architecture to electrochemical performance, the TD-mediated GPT-CRISPR platform was compared with a conventional linear DNA probe-mediated CRISPR format under otherwise identical assay conditions. The linear DNA probe format showed an approximately 10-fold higher LoD than the TD-mediated system (Figure S5A), together with a relatively narrower linear dynamic range (3 to 3 × 10^3 copies μL^{-1}) (Figure S5B). We further assessed the stability of the two formats in complex matrices,

https://doi.org/10.1021/acssensors.6c00902
ACS Sens. XXXX, XXX, XXX-XXX

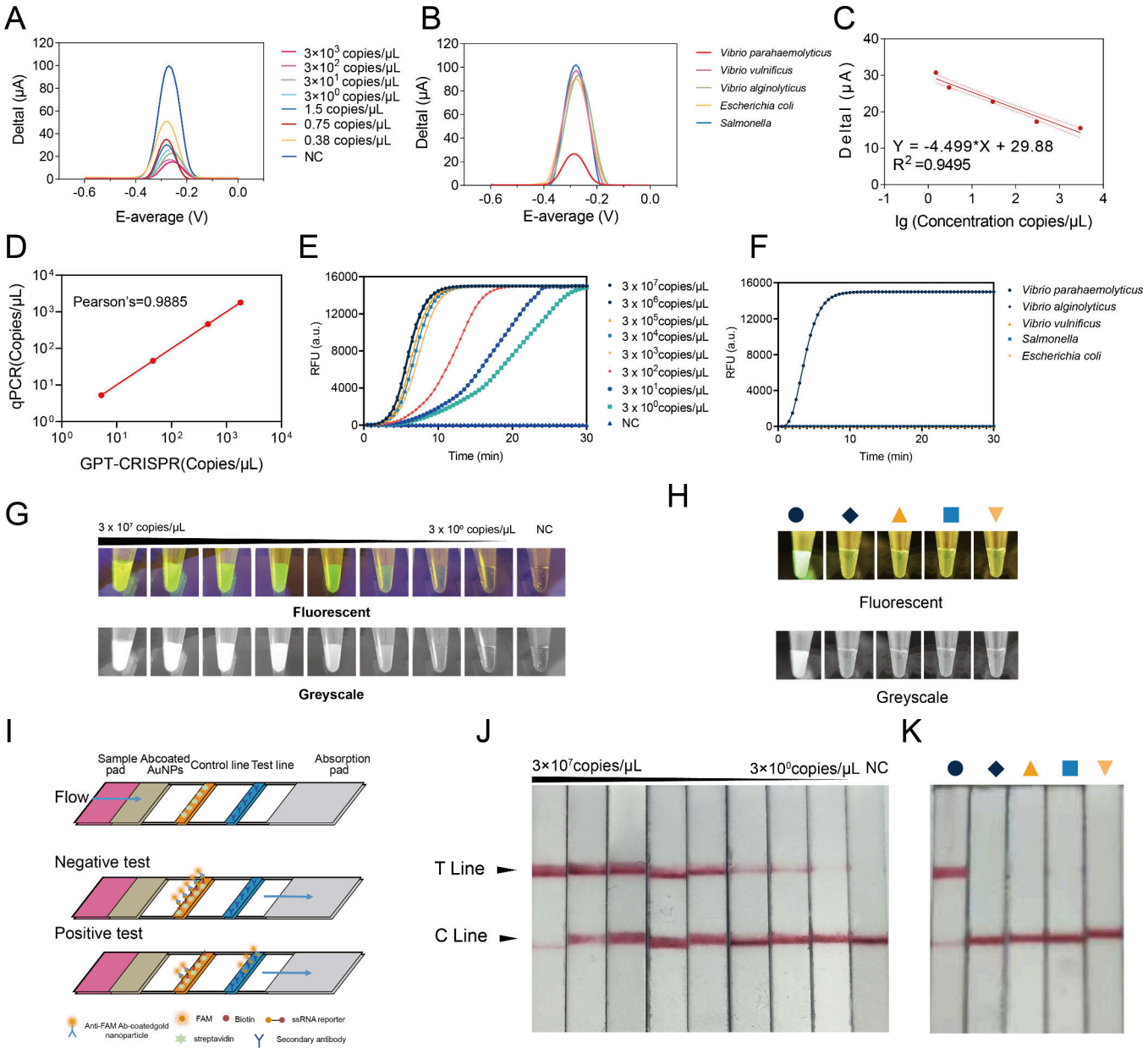


Figure 4. Performance evaluation of the one-pot CRISPR framework with multimodal readouts. (A) Electrochemical signal changes of the TD-mediated interface in response to serial dilutions of VPA1585 plasmid DNA over the range of 3×10^3 to 0.38 copies μL^{-1}. (B) Specificity evaluation of the electrochemical readout using *Vibrio parahaemolyticus* and nontarget bacterial species. (C) Linear relationship between the electrochemical current response and the logarithm of the standard plasmid copy number. (D) Correlation between the GPT-CRISPR results for genomic DNA extracted from serially diluted *Vibrio parahaemolyticus* cultures and the genomic copy numbers determined by qPCR. (E) Sensitivity of the fluorescence readout toward serial dilutions of VPA1585 plasmid DNA (3×10^0 to 3×10^7 copies μL^{-1}). (F) Specificity evaluation of the fluorescence readout using *Vibrio parahaemolyticus* Vp17802 and nontarget bacterial species (*Vibrio alginolyticus* Va2225, *Vibrio vulnificus* Vv-1, *Salmonella* C5004, and *Escherichia coli* ER2738). (G) Blue-light visible endpoint visualization corresponding to the fluorescence sensitivity assay. (H) Blue-light visible visualization corresponding to the fluorescence specificity assay. (I) Schematic illustration of the lateral flow test strip. (J) Sensitivity of the LFA readout toward serial dilutions of VPA1585 plasmid DNA (3×10^0 to 3×10^7 copies μL^{-1}). (K) Specificity evaluation of the LFA readout using *Vibrio parahaemolyticus* and nontarget bacterial species.

including buffer, 3% NaCl APW, pond water, and healthy shrimp tissues. The results showed that the linear DNA probe format exhibited a larger relative standard deviation (RSD = 4.095%) than the TD-mediated GPT-CRISPR platform (RSD = 2.386%) (Figure S5C). In addition, six repeated measurements using independent biosensors indicated relatively lower reproducibility for the linear DNA probe format (RSD = 4.095%) than for the TD-mediated GPT-CRISPR platform (RSD = 2.386%) (Figure S5D). Together, these results support the advantage of the TD-mediated surface-engineered electrochemical interface, which provides more efficient signal amplification and improved analytical performance in the GPT-CRISPR platform.

Specificity was evaluated using genomic DNA from closely related and commonly encountered bacterial species, including *Vibrio*

https://doi.org/10.1021/acssensors.6c00902
ACS Sens. XXXX, XXX, XXX-XXX

alginolyticus, *Vibrio vulnificus*, *Salmonella*, and *Escherichia coli*. Only *Vibrio parahaemolyticus* induced a pronounced decrease in the electrochemical signal, whereas nontarget bacterial species produced responses comparable to the negative control (Figure 4B), confirming the high specificity of the system.

Fluorescence (real-time and endpoint blue-light visualization) (Figure 4E,G) and LFA (Figure 4I,J) readouts were further evaluated. Both formats enabled reliable detection down to 3 copies μL^{-1} (LoD) and provided qualitative or semiquantitative signal outputs. High specificity was also confirmed for both readouts, as no responses were observed for nontarget bacterial species (Figure 4F, H, and K). These complementary readout modes further support the adaptability of the glycine/PVP-enabled one-pot CRISPR framework. Collectively, these results demonstrate that the GPT-CRISPR enables highly sensitive, specific, and quantitative detection of *Vibrio parahaemolyticus*, while the same glycine/PVP-enabled one-pot CRISPR framework can be configured with fluorescence or LFA readouts for flexible deployment.

Detection of *Vibrio parahaemolyticus* in Multiscenario Real Samples

To evaluate the practical applicability of the proposed detection platform, a total of 30 real samples representing five distinct categories were collected, including diseased *Litopenaeus vannamei* samples and aquaculture water from multiple aquaculture farms in Jiangsu Province (China), wastewater from seafood markets, double-blind artificially contaminated samples, and chilled salmon purchased from supermarkets. All samples were analyzed using the established one-pot CRISPR framework with three independent readout formats, including GPT-CRISPR electrochemical sensing (Figure 5A), fluorescence detection (Figure 5B), and LFA (Figure 5C). Quantitative real-time PCR (qPCR) was employed as the reference method, with samples showing Ct values < 35 defined as positive for *Vibrio parahaemolyticus*. Across all 30 samples, the detection results obtained from electrochemical, fluorescence, and LFA readouts were fully consistent with qPCR analysis, yielding a concordance rate of 100%. These

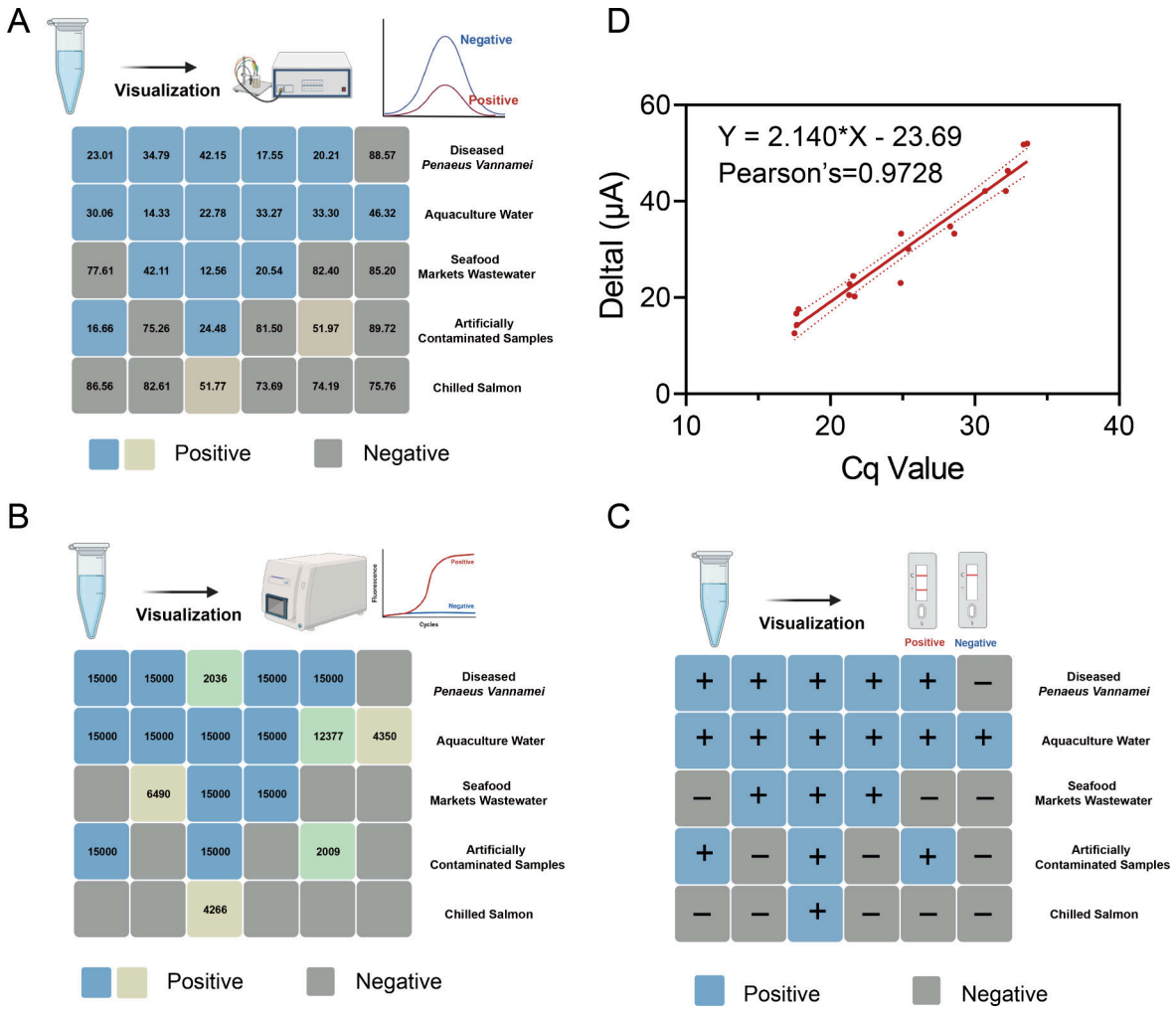


Figure 5. Detection of *Vibrio parahaemolyticus* in multiscenario real samples using the one-pot CRISPR framework. (A) GPT-CRISPR electrochemical detection results for real samples ($n = 6$ per type). Sample type 1: diseased *Litopenaeus vannamei* samples; sample type 2: aquaculture water collected from multiple aquaculture farms in Jiangsu Province (China); sample type 3: wastewater from seafood markets; sample type 4: double-blind artificially contaminated samples; sample type 5: chilled salmon purchased from supermarkets; (B) fluorescence-based detection results for 30 real samples collected from five different sample categories. (C) LFA readout results for the same set of real samples. The upper illustrations in A, B, and C were created using BioRender.com. (D) Correlation analysis between electrochemical signal responses and fluorescence quantitative results for positive samples (Pearson's $r = 0.9728$), demonstrating strong agreement between the two modalities. Heatmaps were generated using locally deployed TBtools-II software.[50]

https://doi.org/10.1021/acssensors.6c00902
ACS Sens. XXXX, XXX, XXX-XXX

results demonstrate that the proposed one-pot CRISPR framework can reliably identify *Vibrio parahaemolyticus* in complex real-world matrices.

To further assess quantitative consistency, correlation analysis was performed between the GPT-CRISPR electrochemical signals and qPCR results for positive samples (Table S4). A strong correlation was observed (Pearson's $r = 0.9728$; Figure 5D), indicating excellent agreement between different detection modalities. Notably, while qPCR required approximately 1 h for completion following bacterial lysis, all three one-pot CRISPR-based frameworks delivered results within 30 min, highlighting the superior speed and field applicability of the proposed platform.

The glycine/PVP-regulated one-pot framework described in this study may be adaptable to a broader range of nucleic acid targets, including pathogens, disease-associated biomarkers, and other diagnostically relevant sequences, provided that the corresponding amplification primers and CRISPR guide RNAs are appropriately redesigned. Thus, the present strategy may not be restricted to *Vibrio parahaemolyticus* detection alone but may offer a generalizable one-pot assay framework for diverse nucleic acid targets. The chemical regulation strategy may also be extendable to other CRISPR-associated nucleases, although this will require further experimental validation. Since the observed effects of glycine and PVP appear to be related mainly to modulation of reaction compatibility and background control within the one-pot system, similar principles may also be relevant to other CRISPR platforms, such as Cas12a. In addition, newly identified nucleases with stronger catalytic activity may potentially be incorporated without altering the core reaction architecture, highlighting the modularity and evolvability of the GPT-CRISPR platform.

Several limitations of the present study should be noted. The assay remains dependent on target-specific primer and crRNA design and thus may require sequence-dependent reoptimization for other applications. In addition, although the electrochemical format provided the best quantitative performance, it still relies on dedicated instrumentation. Moreover, the long-term stability of the regulated one-pot reagents and sensor components has not yet been systematically evaluated. Future work should therefore focus on sequence generalization, instrument simplification, and storage stability to further strengthen the practical utility of the GPT-CRISPR platform.

Overall, these findings suggest that GPT-CRISPR has promising robustness, accuracy, and practical feasibility for diverse target detection, with potential applications in water surveillance, aquaculture, food safety monitoring, and broader molecular diagnostics.

CONCLUSIONS

In summary, we developed a glycine/PVP-enabled one-pot CRISPR sensing framework that integrates chemical regulation of a multienzyme reaction network with tetrahedron-mediated electrochemical transduction for rapid and ultrasensitive detection of *Vibrio parahaemolyticus*. Compared with other reported CRISPR-based assays for *Vibrio parahaemolyticus* detection (Table S5), the present platform integrates glycine/PVP-mediated chemical stabilization, which appears to improve reaction compatibility in a closed one-pot system, with a TD-engineered gold electrode that enables quantitative electrochemical readout of Cas13a activity, achieving a detection limit of 0.38 copies μL^{-1} with a total assay time of less than 30 min.

The framework maintains a unified molecular recognition mechanism while supporting modular readout modes, including electrochemical, fluorescence, and LFA outputs, and shows robust performance in diverse real-world sample matrices. The proposed mechanistic roles of glycine and PVP are based on their reported physicochemical properties and the functional enhancement observed in this study and should therefore be considered functionally supported hypotheses rather than definitive molecular conclusions. Elucidation of the underlying regulation mechanism will be an important direction of our future work.

ASSOCIATED CONTENT

Supporting Information

The Supporting Information is available free of charge at https://pubs.acs.org/doi/10.1021/acssensors.6c00902.

Detailed descriptions of the Experimental Section; optimization of the RAA reaction conditions (Figure S1), optimization of the CRISPR/Cas13a detection system (Figure S2), effects of glycine and PVP (10 kDa) on the fluorescence kinetics of the one-pot CRISPR reaction (Figure S3), characterization of TD nanostructures (Figure S4), comparison of the analytical performance of TD and linear DNA probe interfaces in the GPT-CRISPR platform (Figure S5), and GPT-CRISPR analysis of genomic DNA extracted from serially diluted *Vibrio parahaemolyticus* cultures (Figure S6); primer sequences used for qPCR (Table S1), sequences used for RAA and CRISPR reactions (Table S2), sequences used for DNA tetrahedron assembly (Table S3), qPCR Cq values for clinical samples (Table S4), and summary of reported CRISPR-based detection methods for *Vibrio parahaemolyticus* (Table S5) (PDF)

AUTHOR INFORMATION

Corresponding Author

Xin Zhou – *The First Hospital of Hebei Medical University, Shijiazhuang 050000, China;* Email: zhou_xin@126.com. Tel.: +86-311-87156096

Authors

Jincheng Zhang – *The First Hospital of Hebei Medical University, Shijiazhuang 050000, China; College of Veterinary Medicine, Yangzhou University, Yangzhou 225009, China*

Shuang Liang – *The First Hospital of Hebei Medical University, Shijiazhuang 050000, China; College of Veterinary Medicine, Yangzhou University, Yangzhou 225009, China*

Yue Sun – *College of Veterinary Medicine, Yangzhou University, Yangzhou 225009, China*

Cuixing Zhan – *College of Veterinary Medicine, Yangzhou University, Yangzhou 225009, China*

Gan Xue – *College of Veterinary Medicine, Yangzhou University, Yangzhou 225009, China*

Complete contact information is available at: https://pubs.acs.org/doi/10.1021/acssensors.6c00902

Author Contributions

†J.Z. and S.L. contributed equally to this work. All authors read and approved the manuscript. J.Z., S.L., Y.S., C.Z., and G.X. performed the investigation and data curation. J.Z., S.L., and

https://doi.org/10.1021/acssensors.6c00902
ACS Sens. XXXX, XXX, XXX-XXX

Y.S. contributed to the writing-original draft. J.Z., S.L., and X.Z. contributed to the writing-review and editing. X.Z. contributed to the conceptualization and funding acquisition.

Notes

The authors declare no competing financial interest.

■ ACKNOWLEDGMENTS

This work was supported by the National Fund (no. BWS19C016), start-up funds for high-level talents of the First Hospital of Hebei Medical University, and Postgraduate Research & Practice Innovation Program of Jiangsu Province (grant number SJCX24_2304).

■ REFERENCES

(1) Mclaughlin, J. B.; Depaola, A.; Bopp, C. A.; Martinek, K. A.; Napolilli, N. P.; Allison, C. G.; Murray, S. L.; Thompson, E. C.; Bird, M. M.; Middaugh, J. P. Outbreak of *Vibrio parahaemolyticus* gastroenteritis associated with Alaskan oysters. *N. Eng. J. Med.* **2005**, *353* (14), 1463–1470.

(2) Ndraha, N.; Wong, H. C.; Hsiao, H. I. Managing the risk of vibrio parahaemolyticus infections associated with oyster consumption: a review. *Compr. Rev. Food Sci. Food Saf.* **2020**, *19* (3), 1187–1217.

(3) Roy, P. K.; Roy, A.; Jeon, E. B.; Dewitt, C. A. M.; Park, J. W.; Park, S. Y. Comprehensive analysis of predominant pathogenic bacteria and viruses in seafood products. *Compr. Rev. Food Sci. Food Saf.* **2024**, *23* (4), No. e13410.

(4) Venkatesan, P. Increase in vibrio spp infections linked to climate change. *Lancet Infect. Dis.* **2024**, *24* (1), No. e18.

(5) Kumar, B. K.; Raghunath, P.; Devegowda, D.; Deekshit, V. K.; Venugopal, M. N.; Karunasagar, I.; Karunasagar, I. Development of monoclonal antibody based sandwich ELISA for the rapid detection of pathogenic vibrio parahaemolyticus in seafood. *Int. J. Food Microbiol.* **2011**, *145* (1), 244–249.

(6) Zhou, H.; Liu, X.; Lu, Z.; Hu, A.; Ma, W.; Shi, C.; Bie, X.; Cheng, Y.; Wu, H.; Yang, J. Quantitative detection of vibrio parahaemolyticus in aquatic products by duplex droplet digital PCR combined with propidium monoazide. *Food Control* **2023**, *144*, No. 109353.

(7) Cui, X.; Zhou, H.; Wang, Z.; Yang, J.; Lu, Z.; Shi, C.; Hu, A.; Li, R.; Bie, X. Establishment and application of a multiplex real-time PCR assay coupled with propidium monoazide for the simultaneous detection of viable vibrio parahaemolyticus, vibrio vulnificus and vibrio alginolyticus. *Food Control* **2024**, *158*, No. 110251.

(8) Wang, S.; Gao, Y.; Miao, Y.; Jiang, W.; Zhang, X.; Zheng, Y.; Wang, J.; Zhang, X.; Liao, H.; Li, Y.; et al. Detection of vibrio parahaemolyticus by one-pot LAMP-CRISPR/cas12b combined with immunomagnetic beads. *Food Control* **2025**, *172*, No. 111181.

(9) Wu, H.; Chen, Y.; Yang, Q.; Peng, C.; Wang, X.; Zhang, M.; Qian, S.; Xu, J.; Wu, J. A reversible valve-assisted chip coupling with integrated sample treatment and CRISPR/cas12a for visual detection of vibrio parahaemolyticus. *Biosens. Bioelectron.* **2021**, *188*, No. 113352.

(10) Wu, H.; Qian, S.; Peng, C.; Wang, X.; Wang, T.; Zhong, X.; Chen, Y.; Yang, Q.; Xu, J.; Wu, J. Rotary valve-assisted fluidic system coupling with CRISPR/cas12a for fully integrated nucleic acid detection. *ACS Sens.* **2021**, *6* (11), 4048–4056.

(11) Hu, A.; Kong, L.; Lu, Z.; Zhou, H.; Bie, X. Construction of a LAMP-CRISPR assay for the detection of vibrio parahaemolyticus. *Food Control* **2023**, *149*, No. 109728.

(12) Zhu, H.; Rahman, S. U.; Pan, T.; Yuan, J.; Zhou, X. Dark-field intelligent detection of v Parahaemolyticus using t4 bacteriophage displaying tail spike proteins and gold nanoparticles. *Biosens. Bioelectron.* **2025**, *288*, No. 117830.

(13) Gootenberg, J. S.; Abudayyeh, O. O.; Kellner, M. J.; Joung, J.; Collins, J. J.; Zhang, F. Multiplexed and portable nucleic acid detection platform with cas13, cas12a, and csm6. *Science* **2018**, *360* (6387), 439–444.

(14) Kellner, M. J.; Koob, J. G.; Gootenberg, J. S.; Abudayyeh, O. O.; Zhang, F. Author correction: SHERLOCK: nucleic acid detection with CRISPR nucleases. *Nat. Protoc.* **2020**, *15* (3), No. 1311.

(15) Fozouni, P.; Son, S.; Díaz De León Derby, M.; Knott, G. J.; Gray, C. N.; D'Ambrosio, M. V.; Zhao, C.; Switz, N. A.; Kumar, G. R.; Stephens, S. I.; et al. Amplification-free detection of SARS-CoV-2 with CRISPR-cas13a and mobile phone microscopy. *Cell* **2021**, *184* (2), 323–333.

(16) Lee, I.; Kwon, S. J.; Heeger, P.; Dordick, J. S. Ultrasensitive ImmunoMag-CRISPR lateral flow assay for point-of-care testing of urinary biomarkers. *ACS Sens.* **2024**, *9* (1), 92–100.

(17) Xu, Z.; Chen, D.; Li, T.; Yan, J.; Zhu, J.; He, T.; Hu, R.; Li, Y.; Yang, Y.; Liu, M. Microfluidic space coding for multiplexed nucleic acid detection via CRISPR-cas12a and recombinase polymerase amplification. *Nat. Commun.* **2022**, *13* (1), No. 6480.

(18) Shi, R.; Zhong, L.; Liu, G.; Mak, W. C. CRISPR/cas biosensing technology: from lab assays to integrated portable devices towards wearables. *TrAC, Trends Anal. Chem.* **2024**, *177*, No. 117796.

(19) Zhan, X.; Jiang, Y.; Li, Z.; Hu, X.; Lan, F.; Ying, B.; Wu, Y. Split DNA tetrahedron-mediated spatiotemporal-hierarchy CRISPR cascade integrated with au@pt nanolabels and artificial intelligence for a cervical cancer MicroRNA bioassay. *ACS Nano* **2025**, *19* (25), 22849–22869.

(20) Tian, B.; Wang, Y.; Tang, W.; Chen, J.; Zhang, J.; Xue, S.; Zheng, S.; Cheng, G.; Gu, B.; Chen, M. Tandem CRISPR nucleases-based lateral flow assay for amplification-free miRNA detection via the designed "locked RNA/DNA" as fuels. *Talanta* **2024**, *266* (Pt 1), No. 124995.

(21) Ding, Y.; Huang, Z.; Li, X.; Tang, M.; Li, W.; Feng, S.; Zhao, L.; Zhang, J.; Yuan, S.; Shan, F.; et al. Development of a reverse transcription loop-mediated isothermal amplification based clustered regularly interspaced short palindromic repeats cas12a assay for duck tembusu virus. *Front. Microbiol.* **2023**, *14*, No. 1301653.

(22) Zhao, X.; Wang, Z.; Zhang, H.; Liu, J.; Wu, W.; Yu, L.; Xu, C.; Wang, X.; Hu, Q. Highly sensitive one-pot isothermal assay combining rolling circle amplification and CRISPR/cas12a for aflatoxin b (1) detection. *Anal. Chem.* **2024**, *96* (45), 18070–18078.

(23) Zhang, Y.; Chen, Y.; Zhang, Q.; Liu, Y.; Zhang, X. An am-level sensitive cascade CRISPR-dx system (ASCas) for rapid detection of RNA without pre-amplification. *Biosens. Bioelectron.* **2023**, *230*, No. 115248.

(24) Ackerman, C. M.; Myhrvold, C.; Thakku, S. G.; Freije, C. A.; Metsky, H. C.; Yang, D. K.; Ye, S. H.; Boehm, C. K.; Kosoko-Thoroddsen, T. S. F.; Kehe, J.; et al. Massively multiplexed nucleic acid detection with cas13. *Nature* **2020**, *582* (7811), 277–282.

(25) Li, Z.; Zhao, W.; Ma, S.; Li, Z.; Yao, Y.; Fei, T. A chemical-enhanced system for CRISPR-based nucleic acid detection. *Biosens. Bioelectron.* **2021**, *192*, No. 113493.

(26) Liu, P.; Zeng, J.; Jiang, C.; Du, J.; Jiang, L.; Li, S.; Zeng, F.; Xiong, E. Poly(vinylpyrrolidone)-enhanced CRISPR-cas system for robust nucleic acid diagnostics. *Anal. Chem.* **2024**, *96* (39), 15797–15807.

(27) Wang, Y.; Chen, H.; Gao, H.; Wei, H.; Wang, Y.; Mu, K.; Liu, L.; Dai, E.; Rong, Z.; Wang, S. CESSAT: a chemical additive-enhanced single-step accurate CRISPR/cas13 testing system for field-deployable ultrasensitive detection and genotyping of SARS-CoV-2 variants of concern. *Biosens. Bioelectron.* **2023**, *229*, No. 115238.

(28) Sharma, A.; Faber, H.; Khosla, A.; Anthopoulos, T. D. 3d printed electrochemical devices for bio-chemical sensing: a review. *Mater. Sci. Eng., R* **2023**, *156*, No. 100754.

(29) Umapathi, R.; Ghoreishian, S. M.; Sonwal, S.; Rani, G. M.; Huh, Y. S. Portable electrochemical sensing methodologies for on-site detection of pesticide residues in fruits and vegetables. *Coord. Chem. Rev.* **2022**, *453*, No. 214305.

(30) Wang, S.; Chen, X.; Zhao, C.; Kong, Y.; Lin, B.; Wu, Y.; Bi, Z.; Xuan, Z.; Li, T.; Li, Y.; et al. An organic electrochemical transistor

https://doi.org/10.1021/acssensors.6c00902
ACS Sens. XXXX, XXX, XXX-XXX

for multi-modal sensing, memory and processing. *Nat. Electron.* **2023**, *6* (4), 281–291.
(31) Chen, C.; Chen, S.; Fu, Y.; Wei, Y.; Xie, L.; Chen, M. Electrochemical sensing technology based on a ligation-initiated LAMP-assisted CRISPR/cas12a system for high-specificity detection of EGFR e746-a750 deletion mutation. *Biosens. Bioelectron.* **2024**, *263*, No. 116635.
(32) He, Y.; Jia, F.; Sun, Y.; Fang, W.; Li, Y.; Chen, J.; Fu, Y. An electrochemical sensing method based on CRISPR/cas12a system and hairpin DNA probe for rapid and sensitive detection of salmonella typhimurium. *Sens. Actuators, B* **2022**, *369*, No. 132301.
(33) Wu, C.; Chen, Z.; Li, C.; Hao, Y.; Tang, Y.; Yuan, Y.; Chai, L.; Fan, T.; Yu, J.; Ma, X.; et al. CRISPR-cas12a-empowered electrochemical biosensor for rapid and ultrasensitive detection of SARS-CoV-2 delta variant. *Nano-Micro Lett.* **2022**, *14* (1), No. 159.
(34) Zheng, H.; Wang, Z.; Luo, G.; Du, C.; Zhang, X.; Chen, J. A triple-amplified electrochemical-photoelectrochemical dual-mode biosensing platform for viral gene assay based on catalytic hairpin assembly, CRISPR-cas12a and liposome-entrapped bifunctional methylene blue. *Sens. Actuators, B* **2024**, *411*, No. 135744.
(35) Han, Z.; Wan, F.; Deng, J.; Zhao, J.; Li, Y.; Yang, Y.; Jiang, Q.; Ding, B.; Liu, C.; Dai, B.; et al. Ultrasensitive detection of mRNA in extracellular vesicles using DNA tetrahedron-based thermophoretic assay. *Nano Today* **2021**, *38*, No. 101203.
(36) Li, H.; Han, M.; Weng, X.; Zhang, Y.; Li, J. DNA-tetrahedral-nanostructure-based entropy-driven amplifier for high-performance photoelectrochemical biosensing. *ACS Nano* **2021**, *15* (1), 1710–1717.
(37) Zhan, X.; Jiang, Y.; Lei, J.; Chen, H.; Liu, T.; Lan, F.; Ying, B.; Wu, Y. DNA tetrahedron-enhanced single-particle counting integrated with cascaded CRISPR program for ultrasensitive dual RNAs logic sensing. *J. Colloid Interface Sci.* **2025**, *683* (Pt 2), 521–531.
(38) Xiao, M.; Lai, W.; Man, T.; Chang, B.; Li, L.; Chandrasekaran, A. R.; Pei, H. Rationally engineered nucleic acid architectures for biosensing applications. *Chem. Rev.* **2019**, *119* (22), 11631–11717.
(39) Lin, M.; Song, P.; Zhou, G.; Zuo, X.; Aldalbahi, A.; Lou, X.; Shi, J.; Fan, C. Electrochemical detection of nucleic acids, proteins, small molecules and cells using a DNA-nanostructure-based universal biosensing platform. *Nat. Protoc.* **2016**, *11* (7), 1244–1263.
(40) Wang, S.; Zhang, L.; Wan, S.; Cansiz, S.; Cui, C.; Liu, Y.; Cai, R.; Hong, C.; Teng, I. T.; Shi, M.; et al. Aptasensor with expanded nucleotide using DNA nanotetrahedra for electrochemical detection of cancerous exosomes. *ACS Nano* **2017**, *11* (4), 3943–3949.
(41) Zhang, L.; Jiang, H.; Zhu, Z.; Liu, J.; Li, B. Integrating CRISPR/cas within isothermal amplification for point-of-care assay of nucleic acid. *Talanta* **2022**, *243*, No. 123388.
(42) Li, H.; Kielich, D. M. S.; Liu, G.; Smith, G.; Bello, A.; Strong, J. E.; Pickering, B. S. Strategies to improve multi-enzyme compatibility and coordination in one-pot SHERLOCK. *Anal. Chem.* **2023**, *95* (28), 10522–10531.
(43) Tripathi, R.; Durán Caballero, L.; Pérez De Tudela, R.; Hölzl, C.; Marx, D. Unveiling zwitterionization of glycine in the microhydration limit. *ACS Omega* **2021**, *6* (19), 12676–12683.
(44) Xu, X.; van Haren, M. H. I.; Smokers, I. B. A.; Visser, B. S.; White, P. B.; Jansen, R. S.; Spruijt, E. Amino acids bind to phase-separating proteins and modulate biomolecular condensate stability and dynamics. *Nat. Commun.* **2025**, *16* (1), No. 8723.
(45) Pandya, A.; Zhang, C.; Barata, T. S.; Brocchini, S.; Howard, M. J.; Zloh, M.; Dalby, P. A. Molecular dynamics simulations reveal how competing protein-surface interactions for glycine, citrate, and water modulate stability in antibody fragment formulations. *Mol. Pharm.* **2024**, *21* (11), 5497–5509.
(46) Berwick, R.; Vaux, D. J.; Jean, L. Multiphasic effect of vinyl pyrrolidone polymers on amyloidogenesis, from macromolecular crowding to inhibition. *Biochem. J.* **2018**, *475* (21), 3417–3436.
(47) Matić, M.; Saurabh, S.; Hamacek, J.; Piazza, F. Crowding-induced uncompetitive inhibition of lactate dehydrogenase: role of entropic pushing. *J. Phys. Chem. B* **2020**, *124* (5), 727–734.
(48) Stringer, M. A.; Cubuk, J.; Incicco, J. J.; Roy, D.; Hall, K. B.; Stuchell-Brereton, M. D.; Soranno, A. Excluded volume and weak interactions in crowded solutions modulate conformations and RNA binding of an intrinsically disordered tail. *J. Phys. Chem. B* **2023**, *127* (26), 5837–5849.
(49) Fang, J.; Chen, Q.; Ran, M.; Chen, R.; Chen, W.; Cui, J.; Wang, J.; Zhong, K.; Shi, L.; Lu, C.; et al. RPA-CRISPR/cas12a-coupled microfluidic biosensor enabling on-site, sensitive quantification of vibrio parahaemolyticus. *Biosens. Bioelectron.* **2026**, *296*, No. 118327.
(50) Chen, C.; Wu, Y.; Li, J.; Wang, X.; Zeng, Z.; Xu, J.; Liu, Y.; Feng, J.; Chen, H.; He, Y.; et al. TBtools-II: a "one for all, all for one" bioinformatics platform for biological big-data mining. *Mol. Plant* **2023**, *16* (11), 1733–1742.

https://doi.org/10.1021/acssensors.6c00902
ACS Sens. XXXX, XXX, XXX-XXX